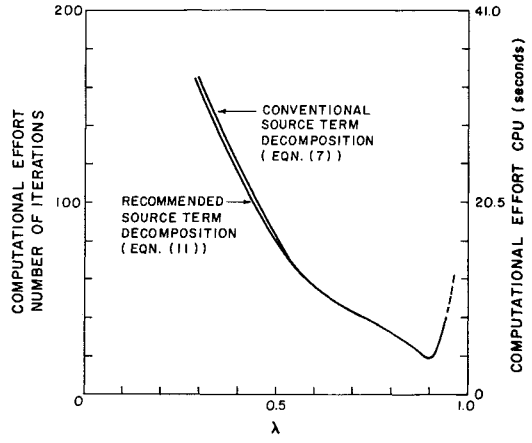

Fig. 3 Comparison of computational effort for swirl number $S = 0.5$.

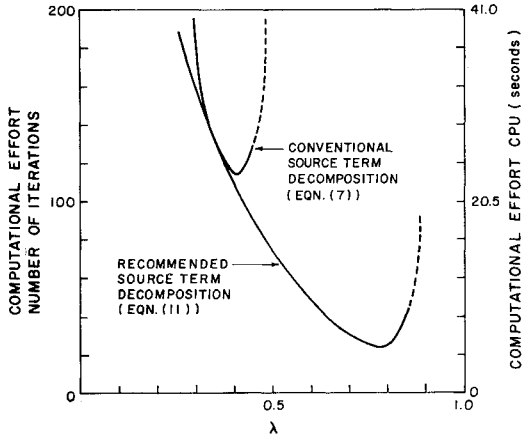

Fig. 4 Comparison of computational effort for swirl number $S = 2.0$.

where $\|r_u\|$ is the Euclidian norm of the residual for u, and it is defined as

$$\|r_u\| = \left[\sum_{C \cdot V} \left(\sum_{nb} a_{nb} u_{nb} + S_C \Delta V_P - \tilde{a}_P u_P \right)^2 \right]^{\frac{1}{2}} \qquad (14)$$

The outer summation in the preceding equation is performed over all the control volumes in the domain.

Results are presented in Fig. 3 for $S = 0.5$, and in Fig. 4 for $S = 2.0$. The computational effort expressed as the number of iterations (shown on the vertical left axis), and the CPU time in seconds (shown on the vertical right axis) are plotted against the under-relaxation factor λ.

At low swirl rates ($S = 0.5$), both the conventional source term decomposition [Eq. (7)] and the source term decomposition recommended in this technical note [Eq. (11)] exhibit similar behavior (Fig. 3). However, at the higher swirl rate ($S = 2.0$), the advantages of the recommended source term decomposition [Eq. (11)] are clearly evident. A five-fold decrease in computational effort is obtained with the source term decomposition proposed in Eq. (11). More importantly, the solution algorithm exhibits stable convergent behavior over a wide range of under-relaxation factors (for λ nearly up to 0.8).

Based on the aforementioned comparisons, it is recommended that in swirling flows the source term decomposition in Eq. (11) should be used. A considerable decrease in the computational effort will be obtained when applied.

Concluding Remarks

A source term decomposition method is proposed, and it is shown to be computationally advantageous in highly swirling flows. The proposed method uses a corrector form of the tangential momentum equation to decompose the source terms of the radial momentum equation.

Acknowledgments

This work was supported by DOW Chemical Company, Plaquemine, LA. Their support is gratefully acknowledged.

References

[1]Raithby, G.D. and Schneider, G.W., "Numerical Solution of Problems in Incompressible Fluid Flow: Treatment of the Velocity–Pressure Coupling," *Numerical Heat Transfer*, Vol. 2, 1979, pp. 417–440.

[2]Van Doormal, J.P. and Raithby, G.D., "Enhancement of the SIMPLE Method for Predicting Incompressible Fluid Flows," *Numerical Heat Transfer*, Vol. 17, 1984, pp. 147–163.

[3]Issa, R.I., Gosman, A.D., and Watkins, A.P., "The Computation of Compressible and Incompressible Recirculating Flows by a Non-iterative Implicit Scheme," *Journal of Computational Physics*, Vol. 62, 1986, pp. 66–82.

[4]Jang, D.S., Jetli, R., and Acharya, S., "Comparison of the PISO, SIMPLER, and SIMPLEC Algorithms for the Treatment of the Pressure–Velocity Coupling in Steady Flow Problems," *Numerical Heat Transfer*, Vol. 10, 1986, pp. 209–228.

[5]Latimer, B.R. and Pollard, A., "Comparison of Pressure–Velocity Coupling Solution Algorithms," *Numerical Heat Transfer*, Vol. 8, 1985, pp. 635–652.

[6]Patankar, S.V., *Numerical Heat Transfer and Fluid Flow*, Hemisphere, New York, 1980.

Passive Venting System for Modifying Cavity Flowfields at Supersonic Speeds

Floyd J. Wilcox Jr.*
NASA Langley Research Center, Hampton, Virginia

Nomenclature

C_D = drag coefficient, based on cavity rear face area, 0.848 in.^{2} (5.47 cm^2)
C_P = pressure coefficient
d = chamber height
h = cavity height, 0.40 in. (1.02 cm)
l = cavity length
M = Mach number

Introduction

EXISTING data available in the literature[1–4] show there are two fundamentally different types of cavity flowfields at supersonic speeds depending primarily on the cavity length-to-height (l/h) ratio. For $l/h \gtrsim 13$, the flowfield expands over the cavity leading edge, attaches to the cavity floor, and exits ahead of the rear face (see Fig. 1). For $l/h \lesssim 11$, the flow passes over the cavity without appreciable deflection. These two flow patterns are generally referred to as closed and open cavity flow, respectively.

A recent experimental investigation[5] has shown that the drag of a cavity with closed flow was substantially higher than that of a cavity with open flow. The higher drag for the closed flow case is due to the large pressure difference between the forward and aft sections of the cavity. In addition, stores

Received Aug. 31, 1987; revision received Oct. 13, 1987.

*Aerospace Engineer, Supersonic/Hypersonic Aerodynamics Branch, High-Speed Aerodynamics Division. Member AIAA.

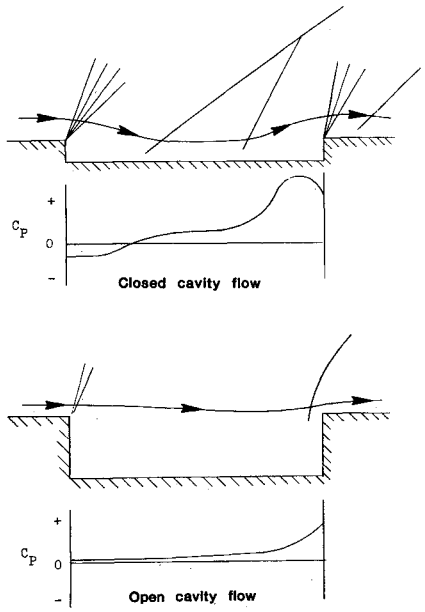

Fig. 1 Cavity flowfield sketches.

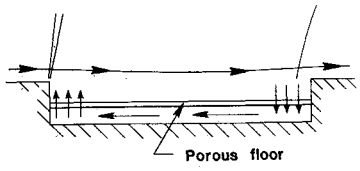

Fig. 2 Porous floor cavity flowfield sketch.

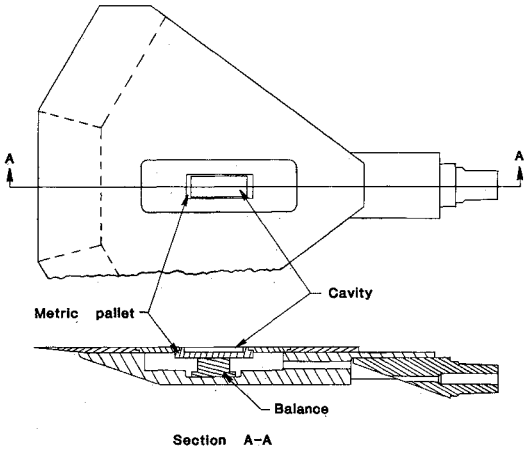

Fig. 3 Flat plate model.

launched from a cavity with closed flow may experience adverse separation characteristics, whereas relatively benign separation characteristics are obtained for open cavity flow.[6] It follows that a passive method to extend the l/h range for which open cavity flow exits would be extremely useful.

The drag of airfoils in transonic flow may be reduced through the use of a passive venting system that uses a porous plate for part of the airfoil upper surface with a vent chamber beneath the porous plate.[7,8] This arrangement allows air from a high-pressure region on the airfoil surface to be vented to a low-pressure region, thereby modifying the airfoil flowfield and resulting in drag reduction. Using this approach, an existing cavity model was modified to house a porous floor with a vent chamber beneath the floor. The expectation was that for closed cavity flow the high-pressure air at the rear of the cavity would vent to the low-pressure region at the front of the

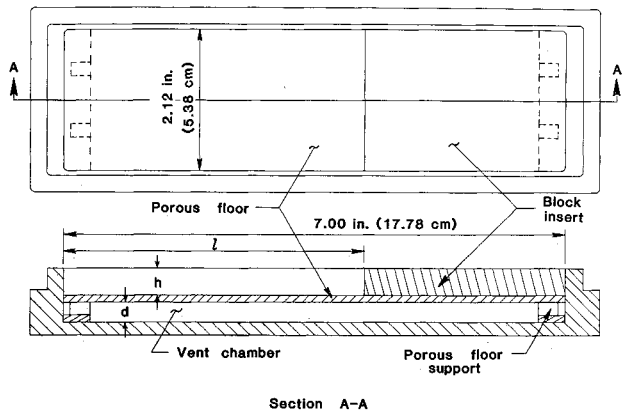

Fig. 4 Cavity pallet details.

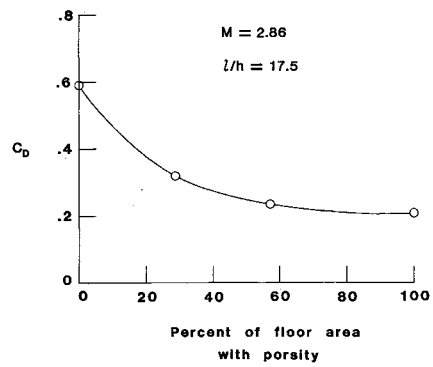

Fig. 5 Effect of porosity on cavity drag.

cavity, causing the flowfield to switch to open cavity flow (see Fig. 2). This Note describes the results of an experimental investigation to determine the effectiveness of this passive venting system.

Experimental Methods

The wind tunnel model consisted of a flat plate, a cavity pallet, and a balance (Fig. 3). The cavity pallet was isolated from the flat plate by a 0.015 in. (0.038 cm) air gap and was mounted on a one-component (axial force) balance such that only the drag of the cavity was measured. A foam rubber seal prevented flow through the air gap. Five static pressure orifices were located on the forward and aft lips of the cavity pallet to correct the drag data for pressure forces on the outside of the pallet. The drag data were also corrected for the tare due to the foam rubber seal and pressure tubes.

Details of the cavity pallet are shown in Fig. 4. Although not shown in the figure, approximately 3340 holes of 0.021 in. diam were drilled in the floor in rows 0.065 in. (0.165 cm) apart with alternating rows containing 31 and 32 holes each. This resulted in a porosity of 7.8% based on the total floor area. A solid floor was simulated by placing adhesive tape over the holes on the vent chamber side of the floor. The cavity height was held constant throughout the entire test while the cavity length was varied by using rectangular block inserts. Estimates of skin friction drag for the top surfaces of the block inserts and pallet were subtracted from the cavity drag measurements. The chamber height could be varied by inserting a filler block into the chamber bottom and replacing the porous floor supports to keep the cavity height constant.

The tests were conducted at Mach numbers of 1.60, 1.90, 2.16, and 2.86 and at a Reynolds number of 2×10^6 ft (6.56×10^6 m). The angle-of-attack of the flat plate was held constant at 0 deg throughout the entire test. Grit type boundary-layer transition strips were applied to the plate leading edge to ensure a fully turbulent boundary layer on the flat plate.

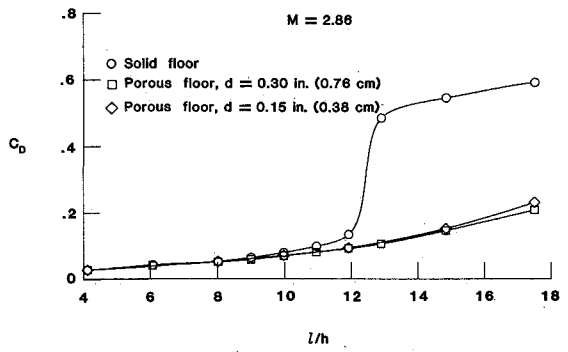

Fig. 6 Effect of porosity in forward and aft sections of cavity floor.

Results

Figure 5 shows results obtained at $M = 2.86$, which were typical of the results obtained at the other Mach numbers. The solid floor data show the typical large drag increase as the cavity flowfield switches from open to closed cavity flow at $l/h \approx 12$. In comparison, the porous floor eliminated the large drag increase for $l/h \gtrsim 12$, suggesting that the flowfield is probably typical of open cavity flow. The chamber height had no effect on the porous floor cavity drag for $l/h \lesssim 12$ and still had a minimal effect for $l/h \gtrsim 12$, although the effect is becoming greater as l/h increases.

Data were also obtained with adhesive tape covering the porous floor symmetrically about the cavity midlength to determine if the porosity near the cavity midlength had a significant effect on the cavity flowfield. Figure 6 shows data for a cavity with $l/h = 17.5$ at $M = 2.86$. The results show a steady decrease in the cavity drag as the percentage of floor area with porosity increases. The solid floor cavity drag was reduced by half when approximately 35% of the floor area was porous. When more than 50% of the floor area was porous, the additional drag reduction obtained was small. Therefore, the porosity near the cavity midlength does not significantly effect the cavity flowfield, i.e., porosity on the forward and aft sections of the cavity floor have the largest effect. This suggests the possibility that other methods (e.g., an array of tubes) could be used to transport the high-pressure air at the rear of the cavity directly to the low-pressure region at the forward part of the cavity and still obtain the same results as the porous floor.

In summary, it has been experimentally shown that a passive venting system can be employed to control cavity flowfields at supersonic speeds. Specifically, the passive venting system has been used to extend the l/h value before the onset of high drag-producing closed cavity flow.

References

[1]Stallings, R.L., Jr. and Wilcox, F.J., Jr., "Experimental Cavity Pressure Distributions at Supersonic Speeds," NASA TP-2683, June 1987.

[2]Kaufman, L.G. II, Maciulaitis, A., and Clark, R.L., "Mach 0.6 to 3.0 Flows Over Rectangular Cavities," AFWAL-TR-82-3112, 1983.

[3]Charwat, A.F., Roos, J.N., Dewey, F.L., Jr., and Hitz, J.A., "An Investigation of Separated Flows—Part I: The Pressure Field," *Journal of Aeronautical Sciences,* Vol. 28, No. 6, June 1961, pp. 457-470.

[4]McDearman, R.W., "Investigation of the Flow in a Rectangular Cavity in a Flat Plate at a Mach Number of 3.55," NASA TND-523, 1960.

[5]Blair, A.B., Jr., and Stallings, R.L., Jr., "Supersonic Axial-Force Characteristics of a Rectangular-Box Cavity with Various Length-to-Depth Ratios in a Flat Plate," NASA TM-87659, April 1986.

[6]Stallings, R.L., Jr., "Store Separations from Cavities at Supersonic Flight Speeds," *Journal of Spacecraft and Rockets,* Vol. 20, March-April 1983, pp. 129-132.

[7]Bahi, L., Ross, J.M., and Nagamatsu, H.T., "Passive Shock Wave/Boundary Layer Control for Transonic Airfoil Drag Reduction," AIAA Paper 83-0137, Jan. 1983.

[8]Nagamatsu, H.T., Orozco, R.D., and Ling, D.C., "Porosity Effect on Supercritical Airfoil Drag Reduction by Shock Wave/Boundary Layer Control," AIAA Paper 84-1682, June 1984.

Base Cavity at Angles of Incidence

Mauri Tanner*
DFVLR—Institute for Theoretical Fluid Mechanics, Göttingen, Federal Republic of Germany

I. Introduction

It is known from several investigations that a base cavity can increase the base pressure and thus decrease the base drag in axisymmetric flow (see Refs. 1-3). However, as far as the author knows, there exist no published results on the effectiveness of a base cavity at angles of incidence. By investigating the influence of tail surfaces on base pressure, some results for a base cavity at angles of incidence were also obtained. These will be given in this paper.

II. Experimental Setup

The measurements were performed in the Transonic Wind Tunnel at Göttingen, which has a test section with a square cross section of 1×1 m^2. The Mach number range is $M_\infty = 0.5$-2.2. The model was an axisymmetric cylinder with an ogival forebody. Its diameter was $D = 45$ mm and its total length $L = 13\,D = 585$ mm. The ogival nose had a length of $1.5\,D = 67.5$ mm. The length of the cylindrical part of the model was, therefore, $11.5\,D = 517.5$ mm. The model was mounted in the wind tunnel by using a sideward strut.

The base cavity used in these measurements has a depth of $T/D = 1.2$. The pressure was measured at eight orifices of 0.6-mm diameter at the bottom of the cavity. On the normal base without a cavity, the pressure was also measured at eight orifices of 0.6-mm diameter. The mean value of these local pressures was denoted as base pressure.

The measurements were performed at Mach numbers from 0.5-1.0. The Reynolds number based on the cylinder diameter was $Re_D = 3.4 \times 10^5$. The angle of incidence had values from $\alpha = 0 - 25$ deg.

III. Results

In Fig. 1, the increase of the base pressure coefficient Δc_{pB} due to the cavity is shown for all Mach numbers investigated at the angle of incidence $\alpha = 0$ deg. The quantity Δc_{pB} is defined by

$$\Delta c_{pB} = (c_{pB})_c - (c_{pB})_n \tag{1}$$

with $(c_{pB})_c$ as the base pressure coefficient for the cavity base and $(c_{pB})_n$ as the base pressure coefficient for the normal base without a cavity. One can see that the base pressure coefficient for all Mach numbers is greater for the cavity base than for the base without a cavity. At $M_\infty = 0.50$, the difference is $\Delta c_{pB} = 0.012$, or about 10% of the base pressure coefficient at the normal base. The increase of the base pressure due to the cavity is smaller for the higher Mach numbers. At $M_\infty = 1.00$, it amounts only to $\Delta c_{pB} = 0.006$, which is about 3.4%.

The investigations of Compton[1] show that the largest increase of the base pressure coefficient due to a base cavity amounts to $\Delta c_{pB} = 0.01$-0.02 at Mach numbers from $M_\infty = 0.3$-1.3. Our new results lie at the lower limit of the values given by Compton.

Morel[2] thoroughly investigated the influence of a base cavity on the base pressure at zero angle of incidence. The base cavities used by Morel had six different depths, namely $T/D = 0.10$, 0.20, 0.35, 0.50, 0.70, and 0.90 (compared with $T/D = 1.20$ as used in the present investigation). The Mach number was $M_\infty = 0.11$, and the Reynolds number based on

Received Feb. 26, 1987; revision received May 8, 1987.

*Research Scientist.